JOURNAL OF AIRCRAFT
Vol. 44, No. 4, July–August 2007

Engineering Notes

ENGINEERING NOTES are short manuscripts describing new developments or important results of a preliminary nature. These Notes should not exceed 2500 words (where a figure or table counts as 200 words). Following informal review by the Editors, they may be published within a few months of the date of receipt. Style requirements are the same as for regular contributions (see inside back cover).

Experimental Evaluation of Sinusoidal Leading Edges

David S. Miklosovic* and Mark M. Murray†
U.S. Naval Academy, Annapolis, Maryland 21402-5042
and
Laurens E. Howle‡
Duke University, Durham, North Carolina 27708-0300

DOI: 10.2514/1.30303

I. Introduction

PREVIOUS studies on increasing airfoil lift and improving stall characteristics have addressed various passive and active approaches to modifying the leading and trailing edge shapes. The passive approaches have covered such methods as rippling the trailing edge, applying serrated-edge Gurney flaps, or modifying the leading-edge (LE) profile [1,2]. Other efforts have effectively eliminated the dynamic stall of an NACA 0012 airfoil by perturbing the LE contour as little as 0.5–0.9% of the chord [3]. Levshin et al. [4] demonstrated that sinusoidal LE planforms on an NACA 63-021 airfoil section decreased maximum lift, but extended the stall angle by almost 9 deg. The larger amplitude sinusoids created "softer" stall characteristics by maintaining attached flow at the peaks despite separated flow in the troughs. These tests were performed to simulate the effects of LE tubercles on humpback whale (*Megaptera novaeangliae*) flippers.

Prior work by the authors also reported wind tunnel measurements for idealized scale models of humpback whale flippers [5]. One model had a smooth leading edge and a second model had sinusoidal bumps (tubercles) along the leading edge for the outer $\frac{2}{3}$ of the span. It was found that the addition of tubercles to a 3-D idealized flipper increased the maximum lift coefficient while reducing the drag coefficient over a portion of the operational envelope. It is thought that the tubercles on the flipper leading-edge enhance the whale's ability to maneuver to catch prey [6]. Though the work to date regarding sinusoidal or serrated leading-edge planforms is largely motivated by marine mammal locomotion, the effects of extending the stall point for lifting surfaces at similar Reynolds numbers (Re) may have application to small-UAV (unmanned aerial vehicle) design and the inevitable laminar stall problems [7]. However other relevant applications might benefit from the effects of simulated tubercles such as stall alleviation/separation control on sailboat centerboards or wind turbines, where an expanded operating envelope could improve the overall effectiveness of the blade [8,9].

In the present work, a better understanding is sought of the mechanism of the improvements measured in previous experiments, with a greater applicability in mind. The authors seek to determine whether the performance improvements resulted from enhancements to the sectional characteristics of wings with tubercles (i.e., essentially 2-D effects), or from Reynolds number effects on a tapered planform, or from other 3-D effects such as spanwise stall progression.

II. Experimental Details

Tests were performed on a full-span model pair and a semispan model pair in two different wind tunnels at the U.S. Naval Academy. Full-span tests were performed at effective Reynolds numbers of 274,000–277,000 and $M_\infty = 0.13$ in a portable, open-return, educational wind tunnel. The test section was 12×12 in. and was instrumented with a three-component internal strain-gage balance. For the models and Reynolds numbers tested, the experimental measurement uncertainty of the balance was demonstrated at an angle of attack (AOA or α) of 4.7 deg. The standard deviation of 30 data points was 0.0045 for the lift coefficient (C_ℓ), 0.0027 for the drag coefficient (C_d), and 0.0017 for the pitching moment coefficient (C_m). These magnitudes doubled as the airfoil entered the stall regime. Semispan tests were conducted at effective Reynolds numbers as high as 534,000–631,000 and $M_\infty = 0.21$ in the U.S. Naval Academy closed circuit wind tunnel. The test section was 54×38 in. and was instrumented with a six-component compact platform balance. The semispan wing models were positioned 0.070 in. above a splitter plate offset 2.25 in. above the tunnel floor. The measurement standard deviation over five digitally integrated datasets was 0.0047 for C_L, 0.0013 for C_D, and 0.0026 for C_M (with the model at $C_{L,\max}$).

All full-span and semispan models were based on the NACA 0020 airfoil profile. The full-span models (Fig. 1a) were fabricated and cured using a 3-D–printing rapid prototyper using an acrylic photopolymer medium. The models had a 3.438 in. chord (c) and an 11.313 in. span which allowed for a 0.125 in. clearance between the wing tips and the test section sidewalls. Spanwise scalloping along the leading edge was introduced using Eq. (1), which yielded a geometric period of 1.435 in. and a scallop amplitude of 4% c. Seven full, spanwise scallops were modeled.

$$x_{\mathrm{LE}} = 0.04\bar{c} \cdot \cos\left(\frac{2\pi \mathrm{y}}{0.41\bar{c}}\right) \tag{1}$$

The semispan models (Fig. 1b) were based on an idealized representation of a specimen humpback whale flipper. They were computer numerical control machined from solid polycarbonate with a half-span of 22.50 in. and $\bar{c} = 5.086$ in. The baseline model had smooth leading and trailing edge planforms defined by Eqs. (2) and (3).

$$x_{\mathrm{LE}} = 2.916 + 0.0624y + 0.000428y^2 - 0.000462y^3 \tag{2}$$

Received 6 February 2007; accepted for publication 30 April 2007.

*Assistant Professor, Aerospace Engineering Department, M.S. 11-B. Member AIAA.
†Assistant Professor, Mechanical Engineering Department, M.S. 11-B.
‡Associate Professor, Mechanical Engineering and Materials Science Department.

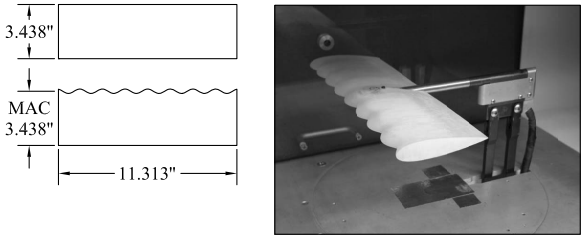

a) Full-span models

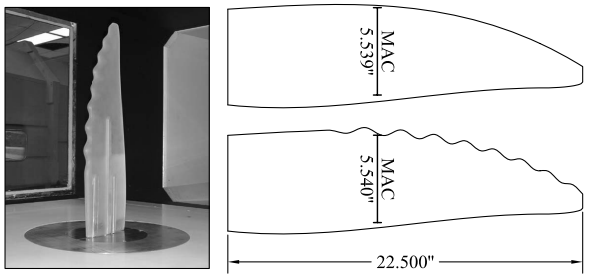

b) Semi-span models

Fig. 1 Wind tunnel models used in the present study.

$$x_{\mathrm{TE}} = \begin{cases} -3.152 - 0.113y + 0.0194y^2 - 0.000552y^3, & y < 19.98 \text{ in.} \\ -0.374\sqrt{1 - 0.158(y - 19.98)^2} - 1.7, & y \geq 19.98 \text{ in.} \end{cases} \tag{3}$$

The semispan scalloped geometry was distinguished by a sinusoidal profile superposed on the leading-edge contour in the spanwise direction. Equation (4) shows the increment that produced the scalloped-LE planform from the smooth one, tapering the amplitude of the sinusoid toward the tip. The largest increment was $\Delta x_{\mathrm{LE}} = \pm 0.223$ in. and it occurred over 39–44% of the half-span.

$$\Delta x_{\mathrm{LE}} = 0.125(1 - 0.001y^2)\sin(0.57y^{1.5} - 0.4)[\tanh(y - 7) + 1] \tag{4}$$

To acquire the data, up to ten samples were acquired and averaged for each data point. Each sample involved a digital integration over an aperture of 20 power line cycles to affect 6.5-digit resolution, as prescribed for high common mode rejection on low-level signals. The force and moment data were corrected for wall interference effects. These included buoyancy, solid and wake blockage (single-pass Maskell method for separated flow), streamline curvature corrections, and downwash corrections (semispan models only) as prescribed in [10]. For the full-span models, the high frontal-area blockage of 10.5% (and a planform-to-tunnel-cross-section ratio of $S/C = 0.28$) produced a corrected velocity that was 6.4% higher than indicated in the deep-stall regime. This resulted in a decrease in C_ℓ of 0.095, an increase in C_d of 0.050, and an increase in C_m of 0.014. The prestall corrections created an increase in AOA of less than 0.2 deg, a decrease in C_ℓ of 0.067, an increase in C_d of 0.002, and an increase in C_m of 0.003. The semispan models had a much lower frontal-area blockage of 2% ($S/C = 0.056$) and a span ratio of 59%. Thus the prestall corrections created at most a 0.3 deg increase in AOA, a decrease in C_L of 0.001, an increase in C_D of 0.004, and a change in C_M of less than 0.0004. The effective velocity through the test section was increased by 1.6%, at most, as a result of solid and wake blockage effects in the poststall regime.

III. Full-Span Results

The full-span tests were used to determine the "quasi-2-D" effects of the sinusoidal leading-edge planform as seen in Fig. 2. Here the experimental data are compared with analytic results for an NACA 0020 airfoil produced by the XFOIL code for a Reynolds number of 270,000 and a free transition criterion of $n_{\mathrm{crit}} = 7$ as described in [11]. Over a Reynolds number range of 270,000–

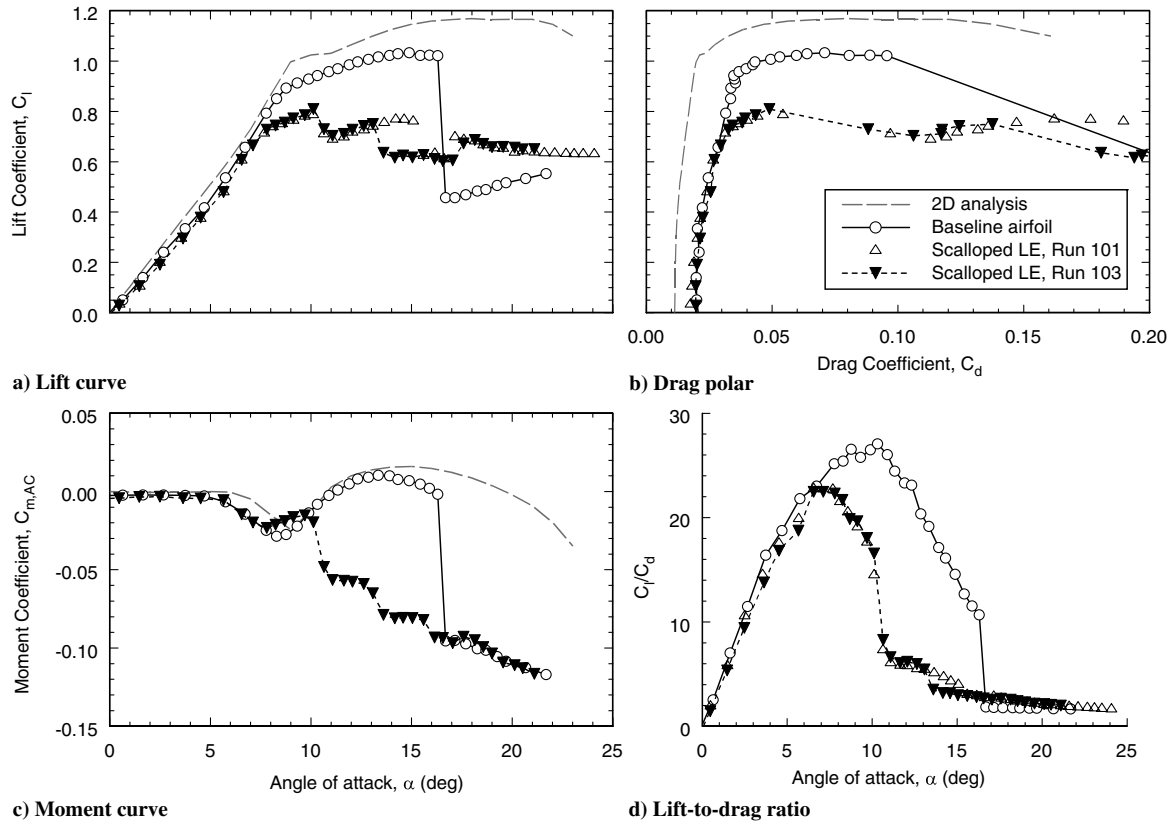

a) Lift curve

b) Drag polar

c) Moment curve

d) Lift-to-drag ratio

Fig. 2 Full-span aerodynamic characteristics.

1,000,000, the 2-D analysis showed that $C_{\ell,\max}$ scaled approximately as $Re^{0.068}$, whereas $C_{d,\min}$ scaled as $Re^{-0.23}$.

The 2-D lift curves in Fig. 2a show that the experimental lift slope (0.0899/ deg) and qualitative C_ℓ trends (including stall progression for the baseline airfoil) were predicted by the 2-D analysis. The differences were due to the relatively large endwall clearance of 0.125 in., an effect exhibited in similar tests performed in this facility. For the baseline, $C_{\ell,\max} = 1.046$ at $\alpha = 16.3$ deg, but this dropped to 0.798–0.810 at 10.1 deg for the two scalloped-LE runs (runs 101 and 103 were taken several days apart to show repeatability). For $\alpha < 7$ deg, the scallops produced essentially the same lift and lift-to-drag ratio (L/D) as the baseline model, but above 8 deg AOA they produced as much as 16% less lift and 17% less L/D (see Fig. 2d). By 10 deg AOA, the scalloped-LE curve broke off in a typical LE stall characteristic, but the loss of lift was only 13% and the airfoil had recovered to $C_\ell = 0.75$ by 15 deg AOA. Furthermore the difference between runs 101 and 103 in the range 13 deg $< \alpha <$ 18 deg revealed an unsteady stall characteristic as a result of the scallops, yet C_ℓ did not drop below 0.61. This observation was accompanied by the fivefold increase in the standard deviation of the sampling of all three load components of the sting balance. It appears that the only "quasi-2-D" improvements the scallops provided is additional lift beyond the point of deep stall for the baseline airfoil.

The drag polars and pitching moment characteristics are compared in Figs. 2b and 2c. The experimental values of C_d were elevated by the presence of the sting pitch mechanism behind the wing and the consequence of the vortex characteristic of the endwall flow. The effect of the sinusoidal LE was to increase the drag for 7 deg $< \alpha <$ 16 deg. Before stall for the baseline airfoil, the lift was 38% lower and the drag 137% higher as a result of the LE scallops. Above the stall point for the baseline airfoil, however, the scallops increased lift by as much as 48% and decreased drag by about 6%. The pitching moment curve (referenced to the aerodynamic center, AC) was matched in characteristic and magnitude between the experimental baseline and the analytic results. The value of $C_{m,\mathrm{AC}}$ decreased sharply at the stall angle, decreasing by 0.09 for the baseline airfoil but only 0.04 for the scalloped-LE airfoil. It was seen that $C_{m,\mathrm{AC}}$ was very agreeable at $\alpha < 8$ deg and $\alpha > 16$ deg for both geometries.

IV. Semispan Results

The semispan tests were used to quantify the 3-D effects of leading-edge scallops on a moderate aspect ratio, high taper ratio wing (see Fig. 3). Here the experimental data are compared with the vortex lattice method of Margason, Lamar, and Herbert [12]. These calculations assumed full LE suction and side-edge attached flow. The analysis was used to model the semispan baseline planform using 26 line segments and 370 horseshoe vortices.

The comparison in 3-D lift is shown in Fig. 3a. These results show that $C_{L,\max} = 0.88$ at $\alpha = 11.9$ deg followed by a marked tip stall behavior for the baseline wing. A strong linearity interrupted by the initial loss in lift of only 13% was indicative of a leading-edge separation as a result of a lower Reynolds number flow regime and/or a small leading-edge radius, but it was confined to the tip region. The plausibility of this assumption is supported by the low taper ratio of 0.148. The stall pattern then propagated toward the root for $\alpha > 11.9$ deg, gradually decreasing to $C_L = 0.43$ at 17.7 deg AOA. This stall characteristic was interrupted by the LE scallops, however, as the maximum lift increased 4% and α_{stall} increased more than 5 deg. Furthermore the lift coefficient was still above 0.5 at 21 deg AOA. The lift and the L/D ratio (Fig. 3d) were virtually identical for $\alpha < 9$ deg, meaning there was no decrease in the peak L/D as a result of the scallops.

The drag polars, shown in Fig. 3b, are supportive of the stall behavior observations. Tip stall for the baseline occurred at $C_D = 0.0529$, where the aerodynamic efficiency was $L/D = 16.6$. The scalloped-LE wing did not show this trend, and $C_D \approx 0.13$ at $C_{L,\max}$ such that $L/D \approx 7$. The crossover point with the baseline occurred at $C_L = 0.83$, above which there was an L/D benefit of the scalloped-LE wing. Therefore the only range where the LE scallops caused a drag increment was $0.70 < C_L < 0.83$ and the increase was at most 44%. While the scalloped wing produced a $C_{D,\min} = 0.0140$

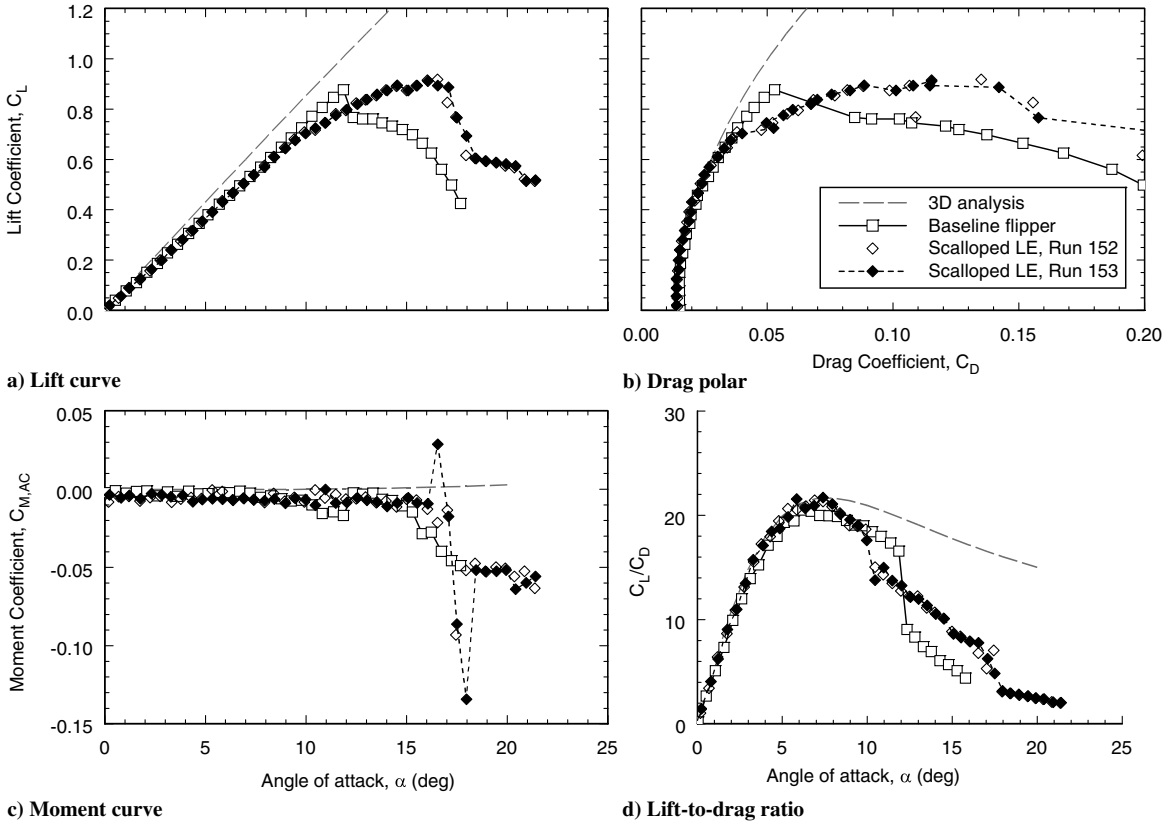

Fig. 3 Semispan aerodynamic characteristics.

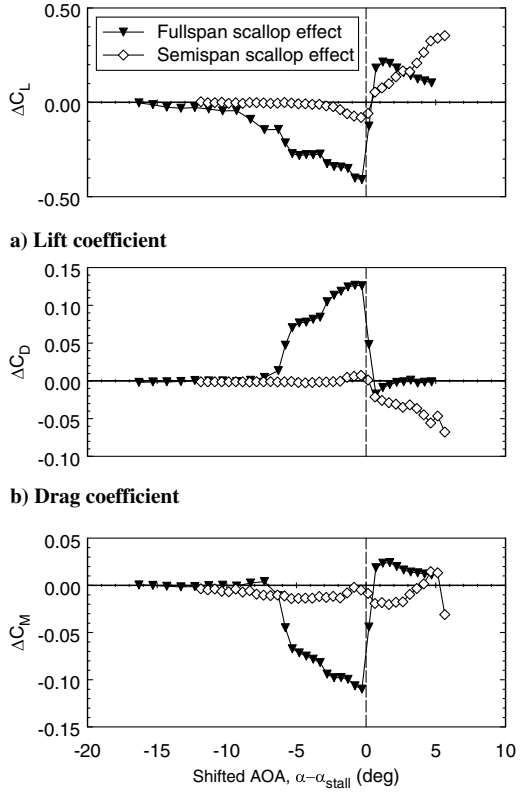

a) Lift coefficient

b) Drag coefficient

c) Pitching moment coefficient

Fig. 4 Incremental effects of sinusoidal leading edges.

compared the baseline of 0.0153, this difference was within the range of measurement uncertainty and is not statistically significant.

The pitching moment (Fig. 3c) showed almost no difference between the baseline and scalloped-LE wings. The curve showed a very flat characteristic with variations in $C_{M,\mathrm{AC}}$ of less than ± 0.01 all the way out to 15 deg AOA. The widely scattered data at 16.5 and 18.0 deg are indicative of the unsteady aerodynamic characteristic as the scalloped wing passed though stall.

V. Discussion

Because of the geometry, the nature of LE scallops is to create an inherently 3-D flow, even over the full-span model. The scallops created a localized variation in LE sweep angle, which defined a spanwise flow component within a cell between scallops. Depending on the local sweep angle, the LE radius, and the AOA, the vortex flow induced localized LE separation and loss of LE suction while at the same time suppressing deep stall somewhat. Evidence of the loss of LE suction was seen in the axial force measurements on the full-span models at $\alpha = 12$ deg: the force coefficient increased from -0.159 to -0.018 due to the LE scallops, revealing less of the forward force that results from LE suction.

The effect of localized LE separation essentially traded higher-efficiency potential lift for lower-efficiency vortex lift. This effect was evident in the change in lift slopes (i.e., the aerodynamic "states") at $\alpha = 8$ deg in Fig. 2a and $\alpha = 10$ deg in Fig. 3a. However the vortical flow induced by the scallops did not produce the same result as traditional vortex generators, which tend to increase both $C_{L,\max}$ and $C_{D,\min}$ together. The characteristic unsteadiness and the elevated lift at high α also pointed to a vortex-dominated flow over the wings with LE scallops.

The "delta" effects of the LE scallops for the 2-D and 3-D geometries are summarized in Fig. 4. Note that the abscissa is the so-called "stall-relative AOA," $\alpha - \alpha_{\mathrm{stall}}$, so that the pre- and poststall effects can be compared. As seen in Fig. 4a, the maximum loss in prestall lift for the semispan wing was 81% lower than the full-span wing; the poststall gains were 65% higher. Figure 4b shows the maximum gain in prestall drag for the semispan wing was only 6% of the full-span drag increment. The poststall drag reduction was enhanced by almost fourfold. For ΔC_M (Fig. 4c), the maximum loss in prestall moment was 88% lower compared with the full-span wing and the poststall gains were 40% lower.

In summary, the vortical flow induced by the sinusoidal LE reduced the effectiveness of the full-span wing by triggering early separation but enhanced the effectiveness of the half-span wing by inhibiting spanwise stall progression thus extending the operating envelope with minimal performance penalties.

VI. Conclusions

Though the aerodynamic mechanisms of the scalloped leading edges are similar, the effects were vastly different between the infinite and finite wings. The substantial loss in lift and increase in drag that accompanied the full-span results, but not the semispan results, means that the scallops had largely a 3-D benefit that is a function of the planform shape and the Reynolds number. At prestall angles of attack, the trends were the same (decrease in lift and moment, increase in drag) but the 3-D effects were much smaller in magnitude. The poststall behavior showed the opposite trends as a result of the scallops: increasing lift and moment, decreasing drag. The generation of vortices by the scallops was beneficial only to 3-D planforms in the range of Reynolds numbers tested. The authors expect that airfoils with tubercles might have utility on lifting surfaces that are required to operate past their stall point, such as wind turbine blades where power generation at lower wind speeds remains a challenge [9]. A flat poststall lift curve as seen in the full-span test results might be beneficial when the blades are operating in the neighborhood of the stall angle for lower speed, unsteady winds.

References

[1] Werle, M. J., Paterson, R. W., and Presz, W. M., "Trailing-Edge Separation/Stall Alleviation," *AIAA Journal*, Vol. 25, April 1987, pp. 624–626.

[2] Gai, S. L., and Palfrey, R., "Influence of Trailing-Edge Flow Control on Airfoil Performance," *Journal of Aircraft*, Vol. 40, No. 2, 2003, pp. 332–337.

[3] Sahin, M., Sankar, L. N., Chandrasekhara, M. S., and Tung, C., "Dynamic Stall Alleviation Using a Deformable Leading Edge Concept: A Numerical Study," *Journal of Aircraft*, Vol. 40, No. 1, 2003, pp. 77–85.

[4] Levshin, A., Custodio, D., Henoch, C., and Johari, H., "Effects of Leading Edge Protuberances on Airfoil Performance," AIAA Paper 2006-2868, June 2006.

[5] Miklosovic, D. S., Murray, M. M., Howle, L. E., and Fish, F. E., "Leading Edge Tubercles Delay Stall on Humpback Whale (Megaptera novaeangliae) Flippers," *Physics of Fluids*, Vol. 16, No. 5, 2004, pp. L39–L42.

[6] Fish, F. E., and Battle, J. M., "Hydrodynamic Design of the Humpback Whale Flipper," *Journal of Morphology*, Vol. 225, No. 1, 1995, pp. 51–60.

[7] Mueller, T. J., and Batill, S. M., "Experimental Studies of Separation on a Two-Dimensional Airfoil at Low Reynolds Numbers," *AIAA Journal*, Vol. 20, No. 4, 1982, pp. 457–463.

[8] Bethwaite, F., *High Performance Sailing*, International Marine, Camden, Maine, 1993.

[9] Hansen, M. O., *Aerodynamics of Wind Turbines*, James & James, London, 2000.

[10] Barlow, J. B., Rae, W. H., and Pope, A., *Low-Speed Wind Tunnel Testing*, 3rd ed., Wiley, Hoboken, NJ, 1999.

[11] Drela, M., and Youngren, H., *XFOIL 6.94 User Guide*, Aeronautical and Astronautical Engineering, MIT, Cambridge, MA, Dec. 2001.

[12] Lamar, J. E., and Herbert, H. E., "Production Version of the Extended NASA-Langley Vortex Lattice FORTRAN Computer Code: Volume I, User's Guide," NASA Tech. Memorandum TM-83303, NASA, 1982.